Charmonium-like states in the $D\bar{D} - D_s\bar{D}_s$ coupled-channel system

Pan-Pan Shi

Institute of Theoretical Physics, Chinese Academy of Sciences

BESIII 粲强子物理研讨会@中国科学技术大学
2023-04-09

PPS, Miguel Albaladejo, Meng-Lin Du, Feng-Kun Guo, Juan Nieves, in preparation.

outline

Exotic states

- Spectrum of mesons on the hidden charm region

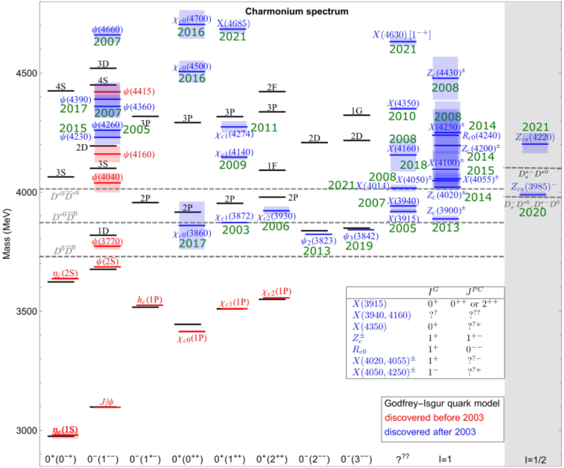

	I^G	J^{PC}
X(3915)	0^+	0^{++} or 2^{++}
X(3940, 4160)	$?^?$	$?^{??}$
X(4350)	0^+	$?^{?+}$
$Z_c^\pm$	1^+	1^{+-}
R_{c0}	1^+	0^{--}
$X(4020, 4055)^\pm$	1^+	$?^{?-}$
$X(4050, 4250)^\pm$	1^-	$?^{?+}$

Categorization of hadrons

- The debates about the nature of exotics still exist

Ordinary hadrons

Exotic hadrons

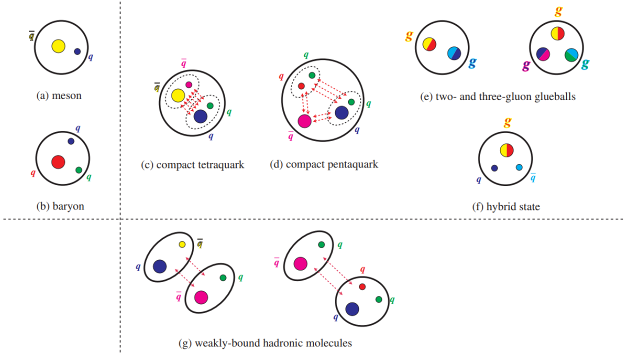

H.-X. Chen, et al., Rept. Prog. Phys. 86 (2023) 2, 026201

$X(3960)$

- LHCb Collaboration obserbed a new state $X(3960)$ in $B^+ \to D_s^+ D_s^- K^+$ process, whose significance is greater than 12 σ LHCb, arXiv:2210.15153, 2211.05034

$$M = (3956 \pm 5 \pm 10)\ \text{MeV}, \quad \Gamma = (43 \pm 13 \pm 8)\ \text{MeV}, \quad J^{PC} = 0^{++}.$$

- $X(3960)$ is a virtual state below $D_s\bar{D}_s$ threshold Teng Ji, et al., PRD 106(2022)094002; arXiv:2212.00631 (2022)
- Based on the $D\bar{D} - D_s\bar{D}_s$ coupled-channel analysis, two bound states are found below $D\bar{D}$ and $D_s\bar{D}_s$ threshold M. Bayar, et al., PRD 107 034007 (2023)
- With the OBE potential, $D^*\bar{D}^*$ and $D_s^*\bar{D}_s^*$ are important to the formation of $X(3960)$ Rui Chen, et al., 2209.05180 (2022)
- $X(3960)$ is a $D_s^+ D_s^-$ molecule with QCD sum rules Qi Xin, et al., AAPPS Bull. 32 (2022) 1, 37; Halil Mutuk, EPJC 82 (2022)12, 1142
- The production $D_s\bar{D}_s$ molecule via the B decay process (10^{-4}) Jia-Ming Xie, et al. Phys.Rev.D 107 (2023) 1, 016003

Lattice Data

	$\lvert\vec{P}\rvert^2$	$\Lambda^{(P)C}$	O	N_{ops}		$\lvert\vec{P}\rvert^2$	$\Lambda^{(P)C}$	O	N_{ops}
O_h	0	A_1^{++}	$\bar{c}c$	7	Dic_4	1	B_1^+	$\bar{c}c$	11
			$D(0)\bar{D}(0)$	2				$D(2)\bar{D}(1)$	1
			$D(1)\bar{D}(1)$	1	Dic_2	2	A_1^+	$\bar{c}c$	28
			$D_s(0)\bar{D}_s(0)$	2				$D(2)\bar{D}(0)$	2
			$D^*(0)\bar{D}^*(0)$	2				$D(1)\bar{D}(1)$	2
			$J/\psi(0)\omega(0)$	2				$D(2)\bar{D}(2)$	1
Dic_4	1	A_1^+	$\bar{c}c$	17				$D(3)\bar{D}(1)$	1
			$D(1)\bar{D}(0)$	2				$D_s(2)\bar{D}_s(0)$	1
			$D(2)\bar{D}(1)$	1				$D_s(1)\bar{D}_s(1)$	1
			$D_s(1)\bar{D}_s(0)$	2				$J/\psi(2)\omega(0)$	3
			$J/\psi(1)\omega(0)$	2					

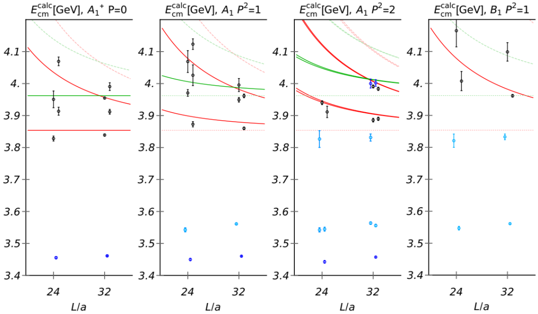

- Single channel:
  $D\bar{D}$ channel: levels n=2(3) from $|\vec{P}| = 0(1)$;
  $D_s\bar{D}_s$ channel: levels n=3, 4 for $|\vec{P}| = 0(1)$ and $N_L = 24$, and n=4, 7 for $|\vec{P}| = 1(2)$ and $N_L = 32$;
- Coupled channel: 14(13) bins for $E_{cm} \approx 3.93 - 4.13$ GeV (n=6 for $|\vec{P}| = 1$ and $N_L = 24$ is dominated by $c\bar{c}^{[J=2]}$).

S. Prelovsek, et al., JHEP 06 (2021) 035.

Poles on the Lattice

- Single channel:
  χ_{c0}^{DD}: $E_B = -4.0^{+3.7}_{-5.0}$ MeV;
  χ_{c2}: $E = 4008^{+14}_{-42} - \frac{i}{2}(64^{+32}_{-42})$ MeV;
- Coupled channel:
  χ'_{c0}: $E = 3983^{+28}_{-20} - \frac{i}{2}(58^{+6}_{-11})$ MeV;
  $\chi_{c0}^{D_sD_s}$:
  $E_B = -0.2^{+0.16}_{-4.9} - \frac{i}{2}(0.27^{+2.5}_{-0.15})$ MeV;

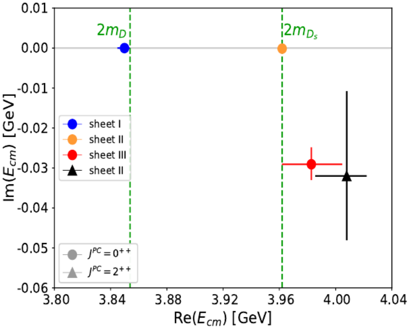

χ_{c2} is likely related to conventional $\chi_{c2}(3930)$ in $L = 2$ $D\bar{D}$ scattering; χ'_{c0} is likely related to $\chi_{c0}(3860)$; $\chi_{c0}^{D_s\bar{D}_s}$ is possibly related to $\chi_{c0}(3930)/X(3915)$.

T-Matrix in the infinite and finite volumes

- T-matrix in infinite and finite volume E. Cincioglu, EPJC 76(2016)10, 576

$$T = F_\Lambda(k)\frac{V(E)}{1-V(E)G(E)}F_\Lambda(k), \quad \tilde{T} = F_\Lambda(k)\frac{V(E)}{1-V(E)\tilde{G}(E)}F_\Lambda(k),$$

with Gaussian matrix of form factor

$$F_\Lambda(k) = \begin{pmatrix} \text{diag}[f_\lambda(k)]_{n\times n} & 0 \\ 0 & 1 \end{pmatrix}, \text{ and } f_\lambda(k) = e^{-k^2/\Lambda}.$$

- Potential for the $D\bar{D} - D_s\bar{D}_s$ coupled-channel system

$$V(E) = \begin{pmatrix} C_{0a} & \frac{\sqrt{2}}{2}(C_{0a}-C_{1a}) & -\frac{\sqrt{3}}{2}d \\ \frac{\sqrt{2}}{2}(C_{0a}-C_{1a}) & \frac{1}{2}(C_{0a}+C_{1a}) & -\frac{\sqrt{3}}{2}d \\ -\frac{\sqrt{3}}{2}d & -\frac{\sqrt{3}}{2}d & 0 \end{pmatrix},$$

The potential includes the contact term and the contribution of a bare charmonium.

- Green's function in the infinite and finite volume

$$G(E) = \begin{pmatrix} [G(E)]_{2\times 2} & 0 \\ 0 & \frac{1}{E^2 - \mathring{m}_{\chi_{c0}}^2} \end{pmatrix}, \tilde{G}(E) = \begin{pmatrix} [\tilde{G}(E)]_{2\times 2} & 0 \\ 0 & \frac{1}{E^2 - \mathring{m}_{\chi_{c0}}^2} \end{pmatrix}.$$

- Green's function in the infinite volume

$$G_{ii}(E) = \int \frac{d^3 q}{(2\pi)^3} \frac{(w_{i1} + w_{i2})\, e^{-2q^2/\Lambda^2}}{2 w_{i1} w_{i2} \left[E - (w_{i1} + w_{i2})^2 + i\epsilon\right]},$$

- Green's function in the finite volume M. Gockeler, et al., PRD 86(2012)094513

$$\tilde{G}^{d}_{ii}(E, L) = \frac{1}{L^3} \sum_{\vec{q}_n \in \Gamma_d} \frac{(\tilde{w}_1 + \tilde{w}_2)\, e^{-2\vec{q}_n{}^2/\Lambda^2}}{2\tilde{w}_1 \tilde{w}_2 \left[E^2 - (\tilde{w}_1 + \tilde{w}_2)^2\right]},$$

where $\Gamma_d = \left\{ \vec{q}_n |\, \vec{q}_n = \frac{2\pi}{L} \left[\vec{n} - \frac{\vec{d}}{2} \left(1 + \frac{m_1^2 - m_2^2}{s} \right) \right], \quad \vec{n} \in \mathbb{Z}^3 \right\}$.

In above, $\tilde{w}_{i1(2)} = \sqrt{\vec{q}^2 + m_{i1(2)}^2}$ and $\tilde{w}_{i1(2)} = \sqrt{\vec{q}_n^2 + m_{i1(2)}^2}$.

Fit the lattice data

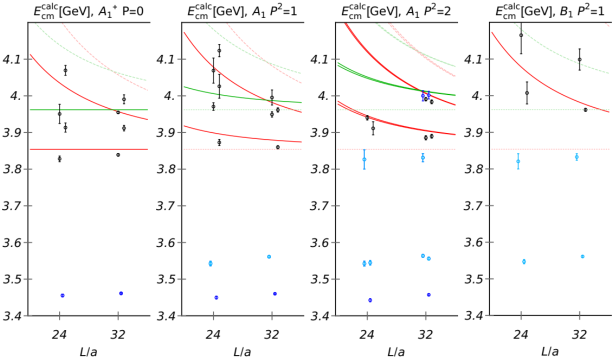

We fit the lattice data with four methods: the lattice data in the rest frame with cutoff $\Lambda = 0.5$ GeV (Fit 1) and $\Lambda = 1.0$ GeV (Fit 2); the lattice data both in the rest and moving frames with cutoff $\Lambda = 0.5$ GeV (Fit 3) and $\Lambda = 1.0$ GeV (Fit 4).

Low energy constants

Table 1: Parameters fitted from lattice data.

	$\overset{\circ}{m}_{\chi_{c0}}$ [GeV]	d [fm$^{1/2}$]	C_{0a} [fm^2]	C_{1a} [fm^2]	χ^2/d.o.f.
Fit 1	$3.95(2)$	$0.77(20)$	$-0.46(48)$	$-0.49(30)$	1.30
Fit 2	$4.06(10)$	$0.57(32)$	$-0.47(22)$	$-0.36(13)$	1.63
Fit 3	$3.99(1)$	$0.35(29)$	$-1.32(30)$	$-0.93(22)$	3.40
Fit 4	$4.11(5)$	$0.36(11)$	$-0.54(7)$	$-0.52(6)$	3.23

- For Fit 1 and Fit 2, the bare masses of charmonium are above the $D_s\bar{D}_s$ threshold about -17 and 97 MeV; For Fit 3 and Fit 4, the bare masses of charmonium are above the $D_s\bar{D}_s$ about 30 and 145 MeV;
- Because of the contribution of bare charmonium ($\sim d^2/[E^2 - (\overset{\circ}{m}_{\chi_{c0}})^2]$), $|C_{0a}|$ is not much larger than $|C_{1a}|$.

Energy levels

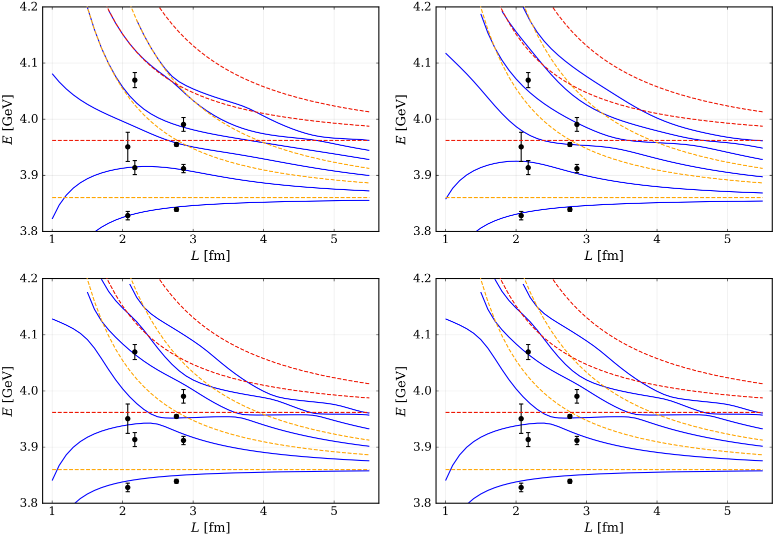

Figure 1: The left (right) panel is relative to $\Lambda = 0.5$ GeV ($\Lambda = 1.0$ GeV).

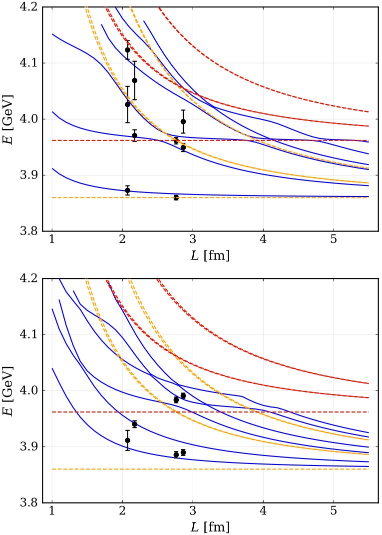

Figure 2: Volume dependence of the energy levels in the moving frame. The left (right) panel is relative to $\Lambda = 0.5$ GeV ($\Lambda = 1.0$ GeV).

Poles in the infinite-volume T-matrix

Table 2: Poles information of the $D\bar{D} - D_s\bar{D}_s$ coupled-channel system for the Fit 1.

Pole [MeV]	$3852.8 - 0i$	$3942.2 - 18.9i$	$4020.1 - 49.2i$	$4006.5 - 42.1i$
RS	$(+,+)$	$(-,+)$	$(-,-)$	$(+,-)$
Channel	Coupling $g_{i,r}$ [GeV]			
$D\bar{D}$	$6.44 + 0i$	$4.55 + 3.28i$	$2.29 + 1.85i$	$3.21 + 1.82i$
$D_s\bar{D}_s$	$4.96 + 0i$	$16.62 + 6.64i$	$3.63 + 5.08i$	$4.06 + 6.30i$
Channel	Weight $P_{i,r}$			
$D\bar{D}$	0.92	0.05	0.01	0.02
$D_s\bar{D}_s$	0.01	-3.75	0.18	0.32

- A bound state below $D\bar{D}$ threshold with $E_B = -1.0$ MeV; a pole on the second RS with binding energy $E_B = -(20 + 18.9i)$ MeV;
- the pole on the fourth RS is a shadow pole of the pole on the third RS. R.J. Eden, et al., Phys.Rev. 133(1964)B1575-B1580.

Table 3: Poles information of the $D\bar{D}-D_s\bar{D}_s$ coupled-channel system for the Fit 2.

Pole [MeV]	$3850.7-0i$	$3969.6-8.3i$	$4125.4-72.1i$	$4090.6-25.1i$
RS	$(+,+)$	$(-,+)$	$(-,-)$	$(+,-)$
Channel	Coupling $g_{i,r}$ [GeV]			
$D\bar{D}$	$8.37+0i$	$0.61+5.80i$	$3.43+3.31i$	$7.05-0.91i$
$D_s\bar{D}_s$	$5.38+0i$	$9.01+7.54i$	$4.12+5.13i$	$7.64+6.20i$
Channel	Weight $P_{i,r}$			
$D\bar{D}$	0.91	0.08	0.03	-0.06
$D_s\bar{D}_s$	0.02	-1.06	0.08	0.01

- A bound state below $D\bar{D}$ threshold with $E_B=-3.1$ MeV; a pole on the second RS with binding energy $E_B=(7.5–8.3i)$ MeV;
- the pole on the fourth RS is a shadow pole.

Table 4: Poles information of the $D\bar{D} - D_s\bar{D}_s$ coupled-channel system for the Fit 3.

Pole [MeV]	$3853.4 - 0i$	$3961.2 - 0.6i$	$4001.9 - 9.5i$	$4000.1 - 6.5i$
RS	$(+,+)$	$(-,+)$	$(-,-)$	$(+,-)$
Channel	Coupling $g_{i,r}$ [GeV]			
$D\bar{D}$	$5.21 - 0i$	$0.91 + 0.52i$	$1.35 + 0.70i$	$1.67 + 0.10i$
$D_s\bar{D}_s$	$1.80 + 0i$	$6.80 + 1.17i$	$2.65 + 3.28i$	$3.22 + 3.32i$
Channel	Weight $P_{i,r}$			
$D\bar{D}$	0.99	0.93×10^{-3}	1.92×10^{-3}	0.57×10^{-3}
$D_s\bar{D}_s$	0.86×10^{-3}	-1.68	0.04	0.03

- A bound state below $D\bar{D}$ threshold with $E_B = -0.4$ MeV; a pole on the second RS with binding energy $E_B = -(1.0 + 0.6i)$ MeV;
- the pole on the fourth RS is a shadow pole.

Table 5: Poles information of the $D\bar{D} - D_s\bar{D}_s$ coupled-channel system for the Fit 4.

Pole [MeV]	$3853.7 - 0i$	$3962.2 - 0.1i$	$4128.3 - 28.3i$	$4124.2 - 6.3i$
RS	$(-,+)$	$(-,+)$	$(-,-)$	$(+,-)$
Channel	Coupling $g_{i,r}$ [GeV]			
$D\bar{D}$	$0 + 3.47i$	$0.12 + 0.65i$	$2.88 + 1.82i$	$3.44 - 1.32i$
$D_s\bar{D}_s$	$0 + 1.02i$	$3.17 + 1.97i$	$3.41 + 3.21i$	$4.13 + 2.98i$
Channel	Weight $P_{i,r}$			
$D\bar{D}$	1.00	0.91×10^{-3}	0.01	-0.01
$D_s\bar{D}_s$	0.02	-1.05	0.01	-0.76×10^{-3}

- A virtual state below $D\bar{D}$ threshold with $E_B = -0.1$ MeV; a pole on the second RS with binding energy $E_B = (0.1 - 0.1i)$ MeV.
- the pole on the fourth RS is a shadow pole.

Summary

- Since the low-energy constants is fitted by lattice data in both rest and moving frames with $\Lambda = 1.0$ GeV, the virtual state is present below $D\bar{D}$ threshold; in other cases, that state is relative to a loosely bound state.
- A pole close to $D_s\bar{D}_s$ threshold is on the 2th Riemann sheet.
- Poles located at 3th and 4th Riemann sheets are above $D_s\bar{D}_s$ threshold. The pole on the 4th Riemann sheet is a shadow pole of the 3th Riemann sheet.

Thanks for your attention!